34th Annual International Conference of the IEEE EMBS
San Diego, California USA, 28 August - 1 September, 2012

Localized Viscoelasticity Measurements with Untethered Intravitreal Microrobots

Juho Pokki[1], Olgaç Ergeneman[1], Christos Bergeles[1,3], Hamdi Torun[2], and Bradley J. Nelson[1]

***Abstract*— Microrobots are a promising tool for medical interventions and micromanipulation. In this paper, we explore the concept of using microrobots for microrheology. Untethered magnetically actuated microrobots were used to characterize one of the most complex biofluids, the vitreous humor. In this work we began by experimentally characterizing the viscoelastic properties of an artificial vitreous humor. For comparison, its properties were also measured using special microcantilevers in an atomic force microscope (AFM) setup. Subsequently, an untethered device was used to study the vitreous humor of a porcine eye, which is a valid *ex-vivo* model of a human eye. Its viscoelasticity model was extracted, which was in agreement with the model of the artificial vitreous. The existing characterization methodology requires eye and vitreous humor dissection for the microrheology measurements. We envision that the method proposed here can be used in *in vivo*.**

I. Introduction

Microrobots are emerging tools for interventions deep in the human body [1]. They have been proposed for kidney stone removal [2], drug delivery through the vasculature [3], and intraocular drug delivery [4]. At these small scales, the interaction of the microrobots and biofluids is a complex research problem, and a good understanding of the properties of the biofluid (e.g., viscosity, flow-rate, elasticity, charges) is needed for evaluation of new swimming techniques, control algorithms, and microrobot designs.

Traditionally, biofluids are studied using methodologies such as optical tweezers, magnetic tweezers, AFM, particle tracking, and microfluidics [5]. The inaccessibility of fluid-filled cavities in the human body, however, makes these methods inapplicable *in vivo*.

One of the most complex fluids in the human body is the vitreous humor, a gel-like water-based fluid (99% H_2O) that contains hyaluronic acid, heterotypic collagen fibrils, and salts. The viscoelastic properties of the vitreous humor have been studied using *ex vivo* human eyes [6] and *ex vivo* porcine eyes [6], [7], [8]. The degradation of the vitreous in *ex vivo* models changes the viscoelastic properties. Additionally, the reported studies involved the dissection of the eye and the removal of the vitreous humor, processes that drastically alter its biomechanics. Recently, [9] used an insertable probe for measurements in an intact eye cavity, but its mechanical interactions with the vitreous humor potentially affected the measurements.

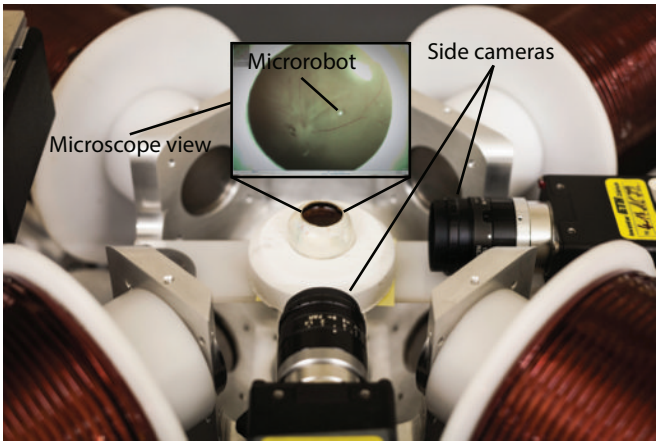

Fig. 1. Experimental setup used to estimate the properties of the porcine vitreous humor. Eight electromagnets (only four are visible) are controlled to generate fields and gradients and apply desired forces and torques on magnetic microdevices.

Magnetic microrobots can be controlled with high precision in 3 dimensions using electromagnetic actuation systems [10]. This high degree of control and the minimally invasive nature of microrobotic interventions motivated us to use simple spherical microrobots and investigate the properties of the vitreous humor in the eye cavity. We experiment with artificial vitreous humor and porcine eyes, comparing our results with parameters extracted by the measurements of an AFM colloidal cantilever. The methodology we propose and evaluate, can be used *in vivo*. This can allow more accurate characterization of the vitreous humor, and, subsequently, the synthesis of better vitreous humor replacements [11].

II. Equipment and Materials

A. Navigation system

For microrobot control, we used a 5 degree-of-freedom electromagnetic control system [10] (see Fig. 1). The system consists of 8 electromagnets arranged in a hemispherical configuration. The separation of the electromagnets respects the anatomy of a small animal (i.e., rabbit) head. By generating magnetic field gradients as in [10], it can propel microrobots through the vitreous humor [4]. Throughout this work the fields were applied at the same direction as the gradients.

Device tracking for position control is achieved using orthogonal cameras [Basler A602fc, Edmund Optics, Germany] (see Fig. 1). Background subtraction, followed by binarization and morphological filtering, detects the device in

This work was supported by the NCCR Co-Me of the Swiss National Science Foundation, and our European Research Council Advanced Grant.

[1]Institute of Robotics and Intelligent Systems, ETH Zurich, 8092 Zurich, Switzerland jpokki at ethz.ch.

[2]Department of Electrical and Electronics Engineering, Boğaziçi University, 34342 Bebek/Istanbul, Turkey.

[3]C. Bergeles is now with Dept. of Cardiovascular Surgery, Children's Hospital Boston, Harvard Medical School, 02115 Boston, MA, USA.

the image. The device's 3D position is calculated via triangulation. During *ex vivo* experiments, the scene is only observable from the top. A microscope [Leica M80, Switzerland] equipped with a camera [Gras-S05C-C, Pointgrey, Germany] records the images, and the 2D position is calculated by scaling. Movement of $>50\,\mu$m ($\simeq$3 pixels) was performed to avoid problems with quantized data.

B. Probes

1) Magnetic NdFeB sphere: A 0.55 mm-diameter NdFeB sphere [Supermagnete, Germany] was used for the viscoelasticity measurements. The magnetic properties of the sphere were measured with a vibrating sample magnetometer [MicroMag, Model 3900]. The magnetic moment of the sphere is $45.53 \pm 0.5\,\mu\text{Am}^2$ at an applied magnetic field of 10 ± 3 mT.

2) Colloidal AFM cantilever probe: A $10\,\mu$m-diameter borosilicate glass bead attached to a silicon-nitride cantilever with a nominal stiffness of 0.01 N/m [Novascan Technologies] was used. The cantilever is soft and the glass bead is a relatively large sphere so that the response to the viscoelasticity is driven mainly by the sphere. Colloidal cantilevers and AFM are commonly used in microrheology to obtain force measurements in viscoelastic fluids [5].

C. Viscoelastic samples

1) Artificial vitreous humor: A vitreous humor phantom was prepared by mixing hyaluronic acid salt (HA, 2.22 mg/mL) and agar (Ag, 1.09 mg/mL) in boiling water (10 mL) [12]. HA gives viscoelastic properties to the solution, and Ag is used to tune the viscosity. The mixture cooled to form a gel-like fluid with viscoelastic properties similar to reported porcine vitreous humor values (i.e., elasticity-related storage modulus G' = 9.8 Pa, and viscosity-related loss modulus G" = 3.9 Pa).

2) Porcine vitreous humor: As an *ex vivo* model, the porcine vitreous humor was examined. Porcine eyes were purchased from a local abattoir. They were stored at $\simeq$5°C and were used within 5 h. The eyes were fixed to a rubber support, and their cornea, iris and lens were carefully removed to expose the vitreous humor. Transscleral illumination through the optic nerve region was applied for high contrast imaging (see Fig. 1). The experiments were conducted with the vitreous humor in the eye globe.

III. Methods

A. Theory

The magnetic force exerted on the sphere is:

$$\mathbf{F}_{\text{magnetic}} = \begin{bmatrix} \frac{\partial \mathbf{B}}{\partial x} & \frac{\partial \mathbf{B}}{\partial y} & \frac{\partial \mathbf{B}}{\partial z} \end{bmatrix}^T \mathbf{M} \tag{1}$$

where $\mathbf{B}$ [T] is magnetic flux density, and $\mathbf{M}$ [A m^2] is the magnetic moment of the sphere. The electromagnetic control system can generate magnetic field gradients up to 1.5 T/m, and, thus, the maximum applicable force on the 0.55 mm-diameter NdFeB bead is $68.30\,\mu$N. Overall:

$$\mathbf{F}_{\text{magnetic}} + \mathbf{F}_{\text{drag}} + \mathbf{W}_{\text{apparent}} = m\,\vec{a} \tag{2}$$

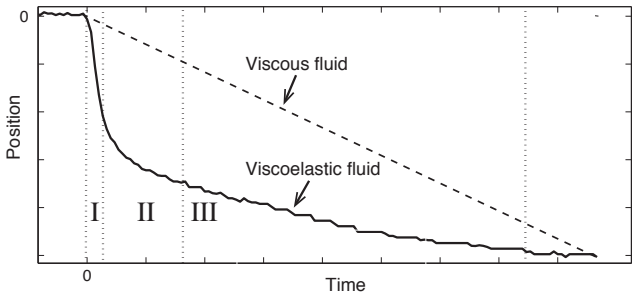

Fig. 2. The position–time response to a constant force on a sphere in a purely viscous (dashed-line), and a viscoelastic fluid (solid line).

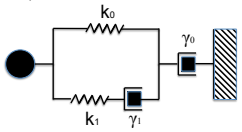

Fig. 3. Kelvin body in a series with a dashpot was applied to model the mechanical behavior in vitreous humor (i.e., time-dependent deflection, or velocity-dependent force). Figure adapted from [13].

where $\mathbf{W}_{\text{apparent}}$ [N] is the apparent weight of the sphere, m [kg] is its mass, and $\vec{a}$ [m s^{-2}] is the acceleration. Knowledge of $\mathbf{W}_{\text{apparent}}$, of $\mathbf{F}_{\text{magnetic}}$ through the output of the magnetic control system, and of $\vec{a}$ through tracking allows the estimation of $\mathbf{F}_{\text{drag}}$ and modeling of the fluid.

B. Viscoelasticity measurements

Figure 2 presents typical time-dependent behavior of a spherical object in a viscoelastic fluid and in a purely viscous fluid in low-Reynolds-number regime under a constant force (i.e., creep). Whereas a constant velocity is maintained in the viscous fluid, the sphere experiences a fast elastic response (I), a relaxation regime (II), and a flow regime (III) in the viscoelastic fluid [13]. Viscoelastic creep measurements allow the extraction of the mechanical properties that arise from the microstructure of the vitreous humor.

The NdFeB sphere was actuated by a stepwise constant magnetic force ($0-13.7\,\mu$N), and its translation was recorded in order to model the time-dependent deflection and obtain the fluid's viscosity and elasticity. As the underlying model of the viscoelastic behavior of the vitreous humor, a Kelvin body in series with a dashpot [13], [14] is considered (see Fig. 3). Under constant force (F), its solution (i.e., viscoelastic creep) of deflection response (p(t)) is:

$$\text{p}(t) = \text{a}\,e^{-\text{b}\,t} + \text{c}\,t + \text{d} \tag{3}$$

where t [s] is time, and a, b, c, and d are tunable model coefficients. The underlying physical model of viscoelasticity is fitted to the data using least-squares method. The steady-state viscosity (γ_0), damping constant (γ_1), effective elasticity ($\text{k} = \text{k}_0 + \text{k}_1$), and relaxation time ($\tau = \text{b}^{-1}$) can be calculated from the coefficients using the following equalities:

$$\begin{aligned} \text{k}_0 &= -\frac{F}{d}, \qquad \gamma_0 = -\frac{F}{c} \\ \text{k}_1 &= \frac{\text{k}_0^2\,a}{F - \text{k}_0\,a}, \quad \gamma_1 = \frac{\tau\,\text{k}_0\,\text{k}_1}{\text{k}_0 + \text{k}_1} \end{aligned} \tag{4}$$

To evaluate the viscoelasticity calculated using the untethered sphere, viscoelastic parameters were also measured separately using a commercial AFM system [Bruker, Dimension Edge, Santa Barbara, CA]. A colloidal probe on a cantilever was immersed in the fluid and constant velocities of the cantilever were recorded (i.e., $\pm 10\,\mu$m/s to $\pm 1000\,\mu$m/s for a deflection of $11\,\mu$m). The entire AFM dataset was fitted to the model of Fig. 3. To simplify analysis and avoid overfitting, k_1 was set to 0. The force response (F [N]) of the cantilever w.r.t. to a constant velocity (v [m/s]) then is:

$$F = \mathrm{k}_0 \ \mathrm{v}\ t + \gamma_1 \mathrm{v} \tag{5}$$

where $\mathrm{k} = \mathrm{k}_0$ is the elasticity, and γ_1 is the damping constant. The elasticity and viscosity parameters from AFM measurements should be in accordance with the results of the spherical-microrobot-based characterization.

IV. Results

A. Artificial vitreous humor

The mechanical properties of the artificial vitreous humor were calculated through measurements from magnetic manipulation (creep data) and AFM. The creep data (i.e., the time-dependent deflection) were collected for two different constant force levels ($F_1 = 2\,\mu$N and $F_2 = 7\,\mu$N) using magnetic control, presented in Fig. 4(a). A combined fit to the creep data was acquired by normalizing the deflection by the force applied ($\frac{p(t)}{F}$) and then fitting the full set of normalized data to (3) using least-squares method with Levenberg-Marquardt algorithm. The fit is shown in Fig. 4(a). Subsequently, the viscosity and elasticity parameters of the artificial vitreous humor were calculated using (4). The results are shown in Table I. The 95% confidence bounds of the viscoelasticity parameters were estimated from the 95% confidence limits of the fit coefficients in (3).

The colloidal AFM probe was excited with varied constant velocities in the artificial vitreous humor, and its force response was recorded. The microcantilever with the probe was calibrated before the AFM experiments. The distance of the bead was kept at $\geq$3 millimeters from the hard surface under the sample to eliminate the wall-effect. The full set of data for the different velocities (see Fig. 4(b)) was fitted to (5) with a root mean square deviation (RMSD) of $0.83\,\mu$N ($\mathrm{R}^2 = 0.897$). The data fitted to the model also allowed the extraction of the viscosity and elasticity parameters of the fluid (see Table I).

Table I shows that the velocity-dependence related damping coefficient (γ_1) was consistent ($\simeq$20% difference) between the AFM and magnetic manipulation methods. Elasticity (k) was on the same order for both methods. The higher elasticity in AFM measurements is possibly due to several reasons. Firstly, traction effects were present on the cantilever, as a fully submerged cantilever will experience forces not only on its tip. As well, the cantilever with a small yet finite stiffness (0.01 N/m, nominal) might contribute to the increased elasticity measured with AFM. The results of Table I indicate the potential of using untethered magnetically actuated microrobots for localized viscoelasticity measurements. Nevertheless, the measurements validate each other and the method of using untethered magnetical microrobots is promising as an advanced microrheometer setup.

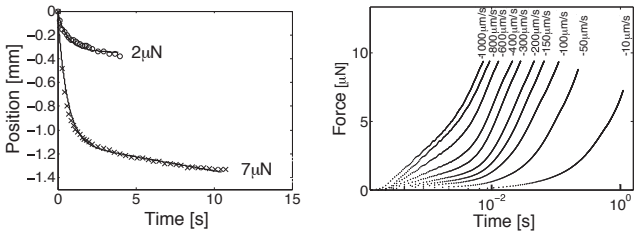

(a) (b)

Fig. 4. (a) Constant magnetic force applied to the NdFeB sphere in the vitreous phantom. The R^2 of the model was 0.978 with a RMSD $< 40\,\mu$m. (b) Force-to-deflection response was recorded for different velocities. The artificial vitreous humor exhibits typical viscoelastic properties such as velocity-dependence.

TABLE I

Elasticity and viscosity parameters for artificial vitreous measurements with 95% confidence bounds.

Coefficient	Magnetic manipulation	AFM
γ_0 [Pa s m]	3.0×10^{-1} $(\pm 0.3 \times 10^{-1})$	NA
γ_1 [Pa s m]	3.8×10^{-3} $(\pm 0.3 \times 10^{-3})$	3.1×10^{-3} $(\pm 0.1 \times 10^{-3})$
k [Pa m]	3.6×10^{-1} $(\pm 0.2 \times 10^{-1})$	9.1×10^{-1} $(\pm 0.1 \times 10^{-1})$
τ [s]	6.1×10^{-1} $(\pm 0.4 \times 10^{-1})$	NA

B. Porcine cadaver vitreous humor

Motivated by the accordance between the two methodologies, we used the untethered sphere to measure the viscosity and elasticity of porcine vitreous humor by conducting similar creep experiments. Fig. 5(a) presents the recorded deflection responses of the sphere to a stepwise constant force ($\pm 2.3\,\mu$N and $\pm 4.6\,\mu$N) in the vitreous humor.

The fitted physical model of Fig. 3 explains the experimental data and is shown in Fig. 5(b) ($\mathrm{R}^2 > 0.9$). Separate fits were conducted for two constant forces. The overall deflection of the sphere with varied applied magnetic forces is presented in Fig. 5(c), and it can be seen that the deflection–force relation is not linear. As seen in Fig. 5(c), there is a minimum force required for the sphere to move. Based on the graph, the minimum force is slightly less than $2.3\,\mu$N, hence, the parameters estimated from the fit of $\pm 4.6\,\mu$N force (R^2=0.966) were more accurate than the parameters estimated from the fit of $\pm 2.3\,\mu$N force (R^2=0.909). In addition, the measurements using $\pm 2.3\,\mu$N force were affected more by quantization of the camera data. Table II presents the steady-state viscosity, damping coefficient, elasticity, and relaxation time for the vitreous humor. These parameters and the parameters calculated for the artificial vitreous humor are in the same range. This is

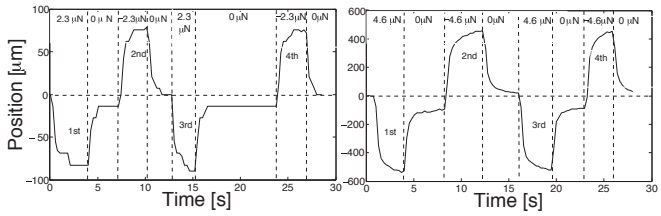

(a) Cycled stepwise constant magnetic force $\pm 2.3\,\mu$N and $\pm 4.6\,\mu$N applied in $\simeq$3-4 s steps to the NdFeB sphere in the center of porcine cadaver vitreous humor.

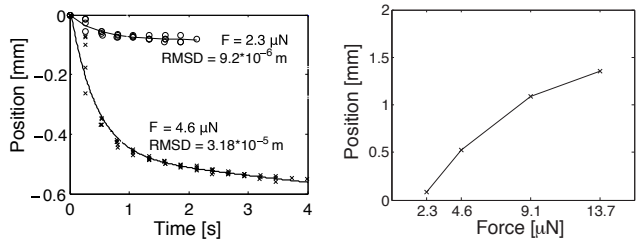

(b) (c)

Fig. 5. Deflection response for different constant forces. (a) Cycled stepwise magnetic force. (b) Deflection (as negative absolute values) for ± 2.3 muN and ± 4.6 muN. (c) Complete deflection for varied force (as absolute values).

TABLE II

ELASTICITY AND VISCOSITY PARAMETERS FROM EX VIVO PORCINE VITREOUS HUMOR MEASUREMENTS WITH 95% CONFIDENCE BOUNDS.

γ_0 **[Pa s m]**	γ_1 **[Pa s m]**	k **[Pa m]**	τ **[s]**
Force 2.3 μN			
6.0×10^{-1} $(\pm7\times10^{-1})$	1.3×10^{-2} $(\pm1.1\times10^{-2})$	8.1×10^{-1} $(\pm4.7\times10^{-1})$	0.42 (±0.35)
Force 4.6 μN			
5.5×10^{-1} $(\pm1.6\times10^{-1})$	0.5×10^{-2} $(\pm0.9\times10^{-2})$	2.4×10^{-1} $(\pm0.3\times10^{-1})$	0.52 (±0.1)

expected since the artificial vitreous humor was synthesized based on porcine vitreous humor parameters.

V. CONCLUSIONS

Researchers already have successfully used magnetically actuated beads to examine and characterize viscoelastic fluids. However, it was not until recently that highly precise magnetic actuation in a large workspace became technically possible. Using an electromagnetic control system able to generate high field gradients in a region that covers the posterior eye segment, we manipulated a permanent magnet sphere to characterize the vitreous humor. The minimally invasive nature of our approach, owing to research conducted for intraocular drug delivery with microrobots, allows the investigation of the vitreous humor in the intact eye cavity. Additionally, the absence of a tether guarantees that the extracted measurements are localized in nature. Previous work was considering the properties of the dissected vitreous humor, or was based on the insertion of a probe in the eye, which causes undesired and hard to quantify traction forces along the probe's shaft.

Our experimental results in artificial vitreous humor show the ability to extract the elasticity and viscosity parameters using an untethered microrobot. The parameters were in agreement with estimates based on AFM-cantilever measurements. As a result, viscoelasticity measurements of the vitreous humor using wirelessly actuated microdevices is a possibility.

Uncertainty is significant in viscoelasticity measurements, and the measurements can have large variations. However, our *ex vivo* experiments demonstrated that we can actuate and measure in the eye cavity without requiring the dissection or extraction of the vitreous humor. The viscosity and elasticity that we calculated were in agreement with the parameters of the artificial vitreous humor.

Given that the utilized electromagnetic control system respects the anatomy of an animal's head, it is possible to teleoperate these microdevices *in vivo* intraocularly. *In vivo* measurements of the parameters of the vitreous humor can lead to improved understanding the properties of the vitreous humor, better vitreous-humor replacements, and advanced designs for intraocular microrobots.

REFERENCES

[1] B. J. Nelson, I. K. Kaliakatsos, and J. J. Abbott, "Microrobots for minimally invasive medicine," *Annual Review of Biomedical Engineering*, vol. 12, pp. 55–85, 2010.

[2] J. Edd, S. Payen, B. Rubinsky, M. L. Stoller, and M. Sitti, "Biomimetic propulsion for a swimming surgical microrobot," *IEEE/RSJ Int. Conf. Intelligent Robots and Systems*, 2003.

[3] S. Martel, O. Felfoul, J. Mathieu, A. Chanu, S. Tamaz, M. Mohammadi, M. Mankiewicz, and N. Tabatabaei, "MRI-based medical nanorobotic platform for the control of magnetic nanoparticles and flagellated bacteria for target interventions in human capillaries," *Int. J. Robotics Research*, vol. 28, no. 9, pp. 1169–1182, 2009.

[4] C. Bergeles, M. P. Kummer, B. E. Kratochvil, C. Framme, and B. J. Nelson, "Steerable intravitreal inserts for drug delivery: *in vitro* and *ex vivo* mobility experiments," *Int. Conf. Medical Image Computing and Computer Assisted Intervention*, pp. 33–40, 2011.

[5] T. A. Waigh, "Microrheology of complex fluids," *Reports on Progress in Physics*, vol. 68, no. 3, pp. 685–742, 2005.

[6] C. S. Nickerson, J. Park, J. A. Kornfield, and H. Krageozian, "Rheological properties of the vitreous and the role of hyaluronic acid," *J. Biomechanics*, vol. 41, no. 9, pp. 1840–1846, 2008.

[7] P. Sharif-Kashani, J. Hubschman, D. Sassoon, and H. P. Kavehpour, "Rheology of the vitreous gel: effects of macromolecule organization on the viscoelastic properties," *J. Biomechanics*, vol. 44, no. 3, pp. 419–423, 2011.

[8] B. Lee, M. Litt, and G. Buchsbaum, "Rheology of the vitreous body: Part 2. viscoelasticity of bovine and porcine vitreous," *Biorheology*, vol. 31, no. 4, pp. 327–338, 1994.

[9] J. A. Zimberlin, J. J. McManus, and A. J. Crosby, "Cavitation rheology of the vitreous: mechanical properties of biological tissue," *Soft Matter*, vol. 6, pp. 3632–3635, 2010.

[10] M. P. Kummer, J. J. Abbott, B. E. Kratochvil, R. Borer, A. Sengul, and B. J. Nelson, "OctoMag: An electromagnetic system for 5-DOF wireless micromanipulation," *IEEE Trans. Robotics*, vol. 26, no. 6, pp. 1006–1017, 2010.

[11] N. Soman and R. Banerjee, "Artificial vitreous replacements," *Biomedical Materials and Engineering*, vol. 13, no. 1, pp. 59–74, 2003.

[12] M. P. Kummer, J. J. Abbott, S. Dinser, and B. J. Nelson, "Artificial vitreous humor for *in vitro* experiments," *IEEE Int. Conf. Engineering in Medicine and Biology*, pp. 6406–6409, 2007.

[13] A. R. Bausch, F. Ziemann, A. A. Boulbitch, K. Jacobson, and E. Sackmann, "Local measurements of viscoelastic parameters of adherent cell surfaces by magnetic bead microrheometry," *Biophysical J.*, vol. 75, no. 4, pp. 2038–2049, 1998.

[14] Y. C. Fung, *Biomechanics - mechanical properties of living tissues*, 2nd ed. New York, USA: Springer, 1993.